Multispacecraft observations of interplanetary shock shapes on the scales of the Earth's magnetosphere

A. Koval[1,2] and A. Szabo[2]

Received 17 February 2010; revised 7 September 2010; accepted 14 September 2010; published 10 December 2010.

[1] We are presenting a study of interplanetary shock shapes as observed by multiple spacecraft in the solar wind. The analysis of the 1 May 1998 shock observed by six spacecraft is presented in detail as an example to demonstrate possible complex shock shapes with small- and large-scale curvatures of the shock surface. To systematically estimate the shock front deviation from planarity on different scales, we are presenting an analysis of 62 shocks observed by Wind and at least one other spacecraft. Our results show the presence of local (on scales up to ~30 R_E) shock curvatures with radii of less than ~50 to ~200 R_E for the majority of analyzed shocks. On larger scales, the shock curvature decreases and reaches the limit of the strongest possible curvature with radius of ~400 R_E on scales greater than ~100 R_E for all analyzed shocks.

Citation: Koval, A., and A. Szabo (2010), Multispacecraft observations of interplanetary shock shapes on the scales of the Earth's magnetosphere, *J. Geophys. Res.*, *115*, A12105, doi:10.1029/2010JA015373.

1. Introduction

[2] The simulation or modeling of the propagation of an interplanetary (IP) shock in the heliosphere, its interaction with planetary magnetospheres, and its particle acceleration effectiveness are dependent on the shock parameters, such as the front orientation, propagation speed, Mach number, and θ_{Bn}, the angle between the shock normal and the magnetic field. Moreover, for a shock moving in the nonuniform solar wind, these parameters are expected to be functions of both time and location, and thus, determination of these parameters at different locations is essential to better characterize the shock.

[3] The shock parameters can be calculated locally from magnetic field and plasma measurements of a spacecraft by fitting the magnetohydrodynamic (MHD) Rankine-Hugoniot (RH) conservation equations to the measurements across a shock. Several such techniques have evolved ranging from simple magnetic coplanarity [*Colburn and Sonett*, 1966], velocity coplanarity [*Abraham-Shrauner*, 1972], and the mixed data methods of Abraham-Shrauner [*Abraham-Shrauner and Yun*, 1976], which use small subsets of RH equations, to sophisticated least squares techniques of *Lepping and Argentiero* [1971] and *Viñas and Scudder* [1986], which use a set of RH equations without temperature terms, namely the mass flux conservation equation, the normal magnetic field continuity equation, the momentum flux conservation equations for the tangential components, and the tangential electric field continuity equations. In contrast to the *Lepping and Argentiero* [1971] technique, where the uniqueness of the solution cannot be established in the multidimensional space of variables, the *Viñas and Scudder* [1986] technique reduces the solution to a self-consistent sequence of one- and two-dimensional least squares problems where the uniqueness of the solution can be demonstrated either analytically or graphically for each step.

[4] *Szabo* [1994] extended the *Viñas and Scudder* [1986] technique by including the momentum flux conservation equation for the normal component and the energy flux conservation equation and included the complete description of possible representations of confidence regions of the solutions. The more recent *Koval and Szabo* [2008] technique is the derivative of the *Viñas and Scudder* [1986] and *Szabo* [1994] technique that finds simultaneous solution for the shock normal and speed, and where the uniqueness of the solution can still be graphically demonstrated in the three-dimensional space.

[5] Since more than one spacecraft measurements are necessary to estimate the shape of an IP shock, only a few studies of shock shapes on the scales of the Earth's magnetosphere have been made. For example, *Russell et al.* [1983a, 1983b] analyzed five IP shocks observed by four spacecraft in the solar wind. In order to find the best fit shock normals at all four spacecraft, they solved an overdetermined set of equations which includes such constrains on normal as separations and time delays between the spacecraft, the field jump at each spacecraft, and the cross product between the upstream (and downstream) magnetic field and the velocity change across the shock. Their comparison of the best fit normals with the solutions of the velocity coplanarity [*Abraham-Shrauner*, 1972] and the mixed data methods of Abraham-Shrauner [*Abraham-Shrauner and Yun*, 1976] suggests that part of the differences may be attributed to the

[1]Goddard Earth Sciences and Technology Center, University of Maryland Baltimore County, Baltimore, Maryland, USA.
[2]Heliospheric Physics Laboratory, NASA Goddard Space Flight Center, Greenbelt, Maryland, USA.

Copyright 2010 by the American Geophysical Union.
0148-0227/10/2010JA015373

real shock orientation variations at different locations. Similarly, *Russell et al.* [2000] analyzed an IP coronal mass ejection (ICME) driven shock on 24 September 1998, which was observed by four spacecraft in the solar wind. To compare different techniques for shock normal and speed determination and to find the most accurate solution, they used the times and locations of the shock observations by the four spacecraft as well as the magnetic field and plasma data before and after the shock measured by three spacecraft. However, they found for the analyzed event that if a 69 s timing (or location) uncertainty is assumed for the IMP 8 measurements, the observations are consistent with a planar shock surface on the spacecraft separation scale.

[6] *Szabo et al.* [2001] showed that with large interspacecraft separation perpendicular to the solar wind flow direction larger angular deviations between individual shock normals are observed. They also analyzed several magnetic cloud (MC) driven shocks to find deviation of the shock shapes from planarity. Their results show that the fast (>600 km/s) and large (>0.25 AU) MCs encountered close to their centers drive nearly planar IP shocks, while IP shocks driven by slow (<400 km/s) and small (<0.2 AU) MCs show a significant level of corrugation. This corrugation appears to be mostly limited to the plane perpendicular to the cloud axis. More recently, *Szabo* [2005a, 2005b] analyzed an ICME-driven shock observed by five spacecraft in the solar wind. Their results suggest that small-scale (few R_E) ripples exist on the surface of the shock.

[7] *Terasawa et al.* [2005] analyzed the IP shock on 29 October 2003 in magnetic field and plasma measurements on Geotail and calculated the shock local orientation using the magnetic field minimum variance analysis and the magnetic coplanarity technique [*Colburn and Sonett*, 1966]. The calculated local shock orientation and speed was used to predict the shock propagation time between Geotail and ACE. The significant difference between the observed and predicted times was suggested to be due to a local shock surface rippling by 15–20° from the "global" surface.

[8] *Neugebauer and Giacalone* [2005] studied the front structure of 26 interplanetary shocks observed by at least five spacecraft. For these shocks, the authors calculated the local shock normals at ACE using the *Viñas and Scudder* [1986] and *Szabo* [1994] technique, and these local normals together with times of shock observations by ACE and other spacecraft were used to calculate the shock curvatures. The obtained curvature radius is in the range from 3×10^5 to 10^7 km, with the average value of 3.5×10^6 km. They also estimated the shock radius of curvature using the calculated shock normals at ACE, Wind, and Geotail, which gave similar results. Consequently, *Neugebauer et al.* [2006] analyzed time-intensity profiles of ~100 keV ions observed by ACE and Wind for 86 shock events. The scale size of persistent particle features in the plane of the shock was estimated to be 2.9×10^6 km, which is similar to the radius of curvature of ripples on the shock surface estimated by *Neugebauer and Giacalone* [2005].

[9] *Pulupa and Bale* [2008] used in situ observations of the source regions of IP type II radio bursts to estimate the structure of IP shock fronts. They analyzed in detail three ICME-driven perpendicular shocks for which Langmuir wave activity and, correlated with it, electron beams in the direction parallel to the interplanetary magnetic field were observed immediately prior to the shock passage. The time difference between the start of the electron flux enhancement, which is an indicator of magnetic connection to a perpendicular shock site, and the shock passage together with the calculated shock speed were used to calculate the shock perpendicular scale, while the electron velocity dispersion allowed calculation of the shock parallel scale. They found for the analyzed events that the local shock curvatures range from a few R_E to a few tens of R_E.

[10] To systematically estimate the shock front deviation from planarity on different scales, we have analyzed in detail 62 IP shocks observed by Wind and at least one other spacecraft in the solar wind at 1 AU. The Wind magnetic field and plasma data were used to calculate the shock local orientation and speed, and these parameters together with the times and locations of the shock observations by two spacecraft allowed the estimation of the shock radius of curvature on the scale of the separation between the spacecraft. Using the measurements of one spacecraft in the estimation of shock curvature, as opposed to comparing the local shock orientations calculated from two or more spacecraft measurements, allows to avoid possible problems of interspacecraft instrument calibrations. The choice of Wind as the main spacecraft was due to the availability of two plasma instruments (3DP and SWE) with different time resolutions, which together provide proton, alpha-particle, and electron measurements, including proton and electron temperature anisotropies. To calculate the shock local parameters at Wind, we used a program with a graphical user interface, which we developed in the Interactive Data Language (IDL), that allows fast and intuitive shock parameter determination from measurements of a number of spacecraft. The program includes the original *Viñas and Scudder* [1986] and *Szabo* [1994] and *Koval and Szabo* [2008] techniques, which assume temperature isotropy, as well as our modifications of these techniques that account for the temperature anisotropy.

[11] As an example of possible complex shock shapes, in section 2 we discuss in detail the IP shock on 1 May 1998 observed by six spacecraft in the solar wind. The statistics of the shapes of 62 IP shocks is presented in section 3, while in section 4 we summarize the results.

2. An IP Shock on 1 May 1998

[12] On 1 May 1998 an ICME-driven shock was observed by six spacecraft located in the solar wind in the range from the L1 point to the Earth's bow shock. The times and locations of the shock observations are summarized in Table 1, and the projections of the spacecraft locations on the XY_{GSE} and XZ_{GSE} planes are also shown in Figure 1.

[13] Figure 2 shows the Wind measurements of the magnetic field (MFI) [*Lepping et al.*, 1995], proton number density and bulk velocity (3DP) [*Lin et al.*, 1995], and proton (3DP) and electron (SWE) [*Ogilvie et al.*, 1995] temperatures that correspond to the shock passage. The changes of the parameters across the shock indicate that the observed shock is a fast forward shock. To calculate the local shock parameters at Wind, the *Viñas and Scudder* [1986] and *Szabo* [1994] technique was applied to the

Table 1. Times and Locations in GSE Coordinates of the Shock Observations on 1 May 1998

Spacecraft	Time (UT)	X (R_E)	Y (R_E)	Z (R_E)
SOHO	2114:30	251.1	71.9	−16.5
Wind	2121:24	215.9	3.9	25.9
ACE	2122:35	228.7	−33.5	−15.6
Interball-1	2154:06	13.7	3.5	10.3
Geotail	2154:25	14.0	21.1	−3.1
IMP 8	2155:50	8.1	30.5	−22.2

magnetic field and plasma measurements. The resulting parameters are: $\phi = 179° \pm 1.3°$, $\theta = 6.0° \pm 0.8°$, $V_S = 640.8 \pm 2.0$ km/s, $M_f = 2.2 \pm 0.3$, $\theta_{Bn} = 28.8° \pm 9.5°$, where ϕ and θ are the shock normal longitude and latitude in GSE coordinates, respectively, V_S is the shock speed, M_f is the fast magnetosonic mach number, and θ_{Bn} is the angle between

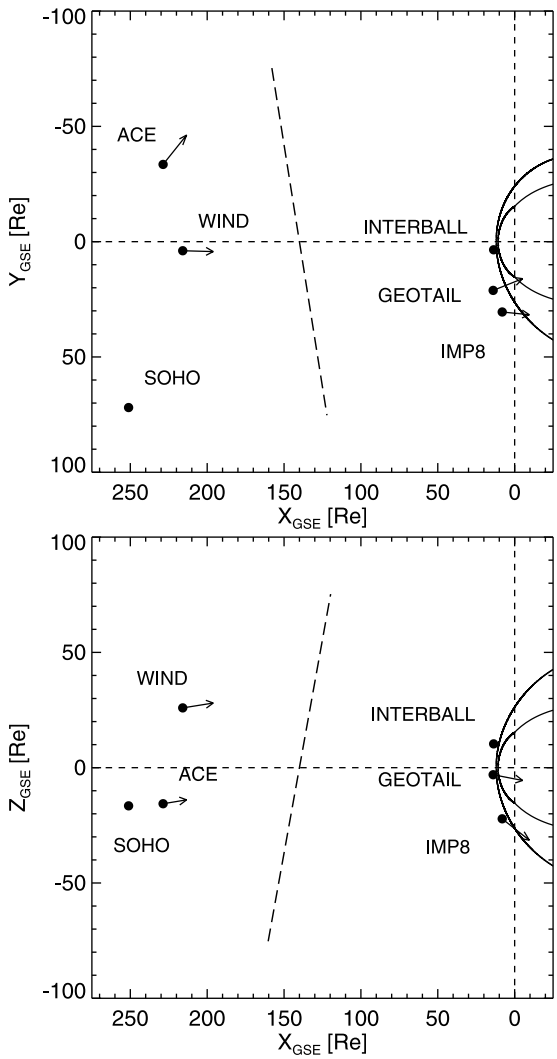

Figure 1. Locations of the spacecraft observing the shock on 1 May 1998. The arrows show the local shock orientations at different locations, while the dashed lines show the global orientation estimated from a four-spacecraft timing. The plotted bow shock and magnetopause are based on the *Jeřáb et al.* [2005] and *Petrinec and Russell* [1996] models, respectively.

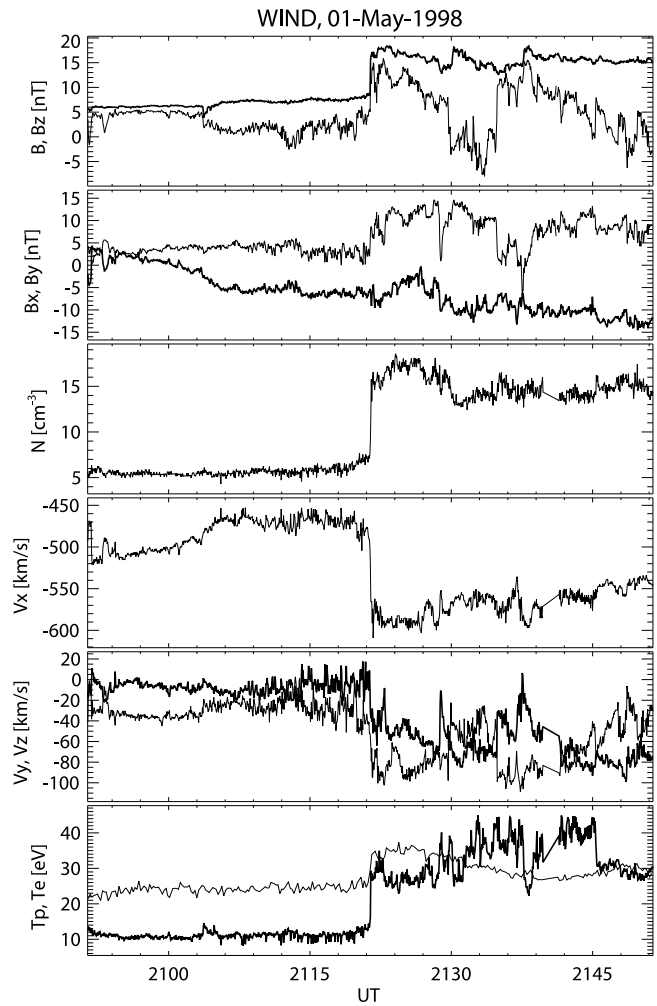

Figure 2. A fast forward IP shock observed by Wind on 1 May 1998. The panels show the magnetic field (MFI), proton number density and bulk velocity (3DP), and proton (3DP) and electron (SWE) temperatures. Vector quantities are in GSE coordinates. For panels with two parameters, the heavy line corresponds to the first parameter.

the shock normal and the magnetic field. Due to the existence of two directions normal to a surface, we assign the shock normal direction to be the one with negative X_{GSE} component.

[14] Of the other five spacecraft observing the shock in the solar wind, SOHO does not possess a magnetic field instrument, while Interball-1 has a data gap in the magnetic field measurements. This precludes from calculating the local shock parameters at these spacecraft; however, we used the SOHO CELIAS/MTOF [*Ipavich et al.*, 1998] and Interball-1 VDP [*Šafránková et al.*, 1997] plasma measurements to identify the shock arrival times. Other three spacecraft, namely ACE, Geotail, and IMP 8, have both magnetic field and plasma measurements necessary for the shock parameter calculation. Figure 3 shows ACE [*Smith et al.*, 1998], Geotail [*Kokubun et al.*, 1994], and IMP 8 [*Mish and Lepping*, 1976] magnetic field profiles across the shock. As can be seen from the data, the magnetic field components differ from one spacecraft to another. This is especially visible when comparing the ACE and other spacecraft

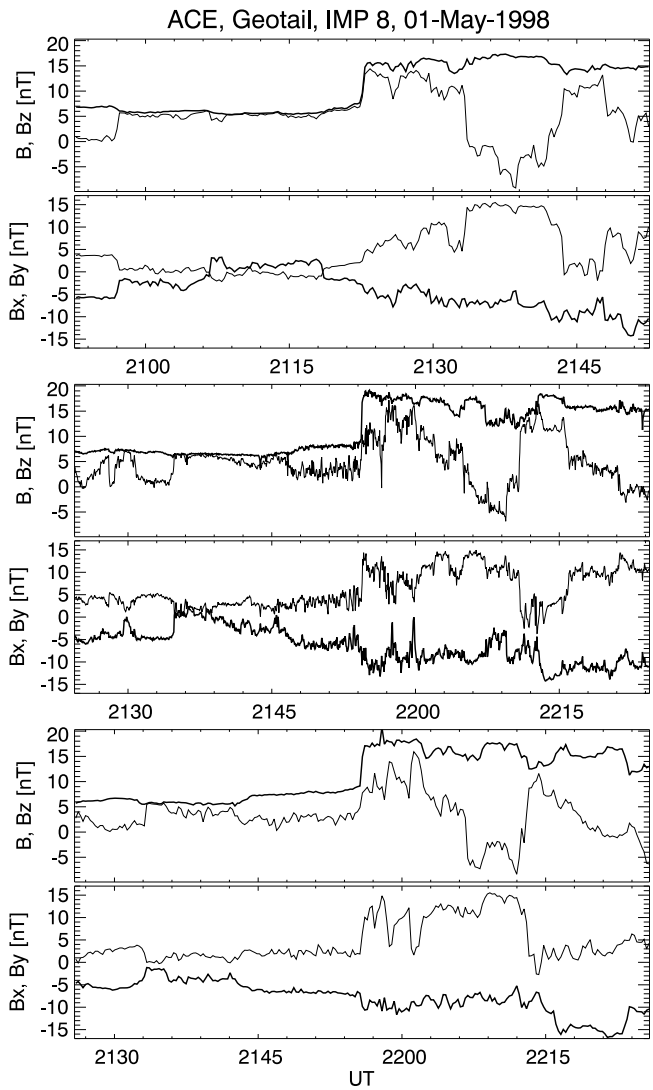

Figure 3. Magnetic field profiles across the 1 May 1998 shock measured by ACE (first and second panels), Geotail (third and fourth panels), and IMP 8 (fifth and sixth panels). For each panel, the heavy line corresponds to the first parameter.

observations. Comparison of plasma parameters (not shown here) indicates significant, although not as high as in the case of magnetic field, differences between the spacecraft. These magnetic field and plasma differences show that the shock propagates in a highly nonuniform solar wind, and these differences are expected to result in significant differences in the calculated local shock parameters.

[15] We applied the same *Viñas and Scudder* [1986] and *Szabo* [1994] technique to the magnetic field data and the ACE SWEPAM [*McComas et al.*, 1998], Geotail CPI [*Frank et al.*, 1994], and IMP 8 MIT Plasma [*Bellomo and Mavretic*, 1978] measurements to calculate the local shock parameters at these spacecraft. The resulting shock normals and speeds are summarized in Table 2, and the normals are also shown by arrows at the corresponding spacecraft locations in Figure 1. The calculated local normals significantly differ in their orientations: the Wind normal points almost along the Sun-Earth line, the ACE normal is highly inclined (≈40°) in the XY_{GSE} plane, and the IMP 8 normal is highly inclined (≈28°) in the XZ_{GSE} plane. Significant differences are also observed between the local shock speeds. It should be pointed out that the calculated shock speed depends on both the calculated shock normal and the plasma measurements on both sides of the shock. If the shock normals differ significantly among the spacecraft, the calculated shock speeds are also expected to differ significantly, even though the plasma parameter differences can be relatively small. This is, for example, the case of high difference between the Wind and ACE shock speeds, as shown in Table 2.

[16] Another test of the shock planarity can be made by comparing the solutions of the four-spacecraft timing technique [*Russell et al.*, 1983a]. Figure 4 shows 15 independent solutions for our case of six-spacecraft observations. The solutions denoted by grey correspond to the spacecraft combinations excluding IMP 8, which may have significant, but unknown, orbit and/or time uncertainties [*Russell et al.*, 2000]. A significant spread of the remaining four-spacecraft solutions, which is not eliminated by excluding the IMP 8 spacecraft, confirms the deviation of the shock shape from planarity.

[17] To further differentiate between the global shock curvature and local ripples on the shock surface, we estimated the shock curvature as a function of the separations between Wind and other spacecraft. For this, the local shock normal and speed at Wind and the times and locations of the shock observations by Wind and other spacecraft were used. Under the assumption that the Wind shock normal and speed are conserved during the time intervals between the shock observations by Wind and other spacecraft, the shock at Wind was propagated to the time when it was observed by the other spacecraft. This provides two points on the shock surface and the shock orientation at one point, which, under assumption of constant shock curvature on the separation between the spacecraft, allows the unique calculation of the radius of curvature or, equivalently, the angle between the normals at two locations on the shock surface. The results are presented in Table 3, which includes the difference between the observed and predicted times of the shock propagation between the two spacecraft ($t_{obs} - t_{pred}$), the spacecraft separation in the direction perpendicular to the normal ($R_{\perp}$), and the estimated angle between the normals at the two locations (α). The last column shows the actual angle between the normals calculated locally at Wind on one side and at ACE, Geotail, and IMP 8 on the other side (see Table 2). As can be seen from the α angles, the Wind normal and speed are in good agreement with the shock observations by all other spacecraft with an exception of ACE. This implies that the shock shape may be close to planarity on the scale of the separation between Wind on the

Table 2. Local Normal Directions in GSE Coordinates and Speeds Calculated From Spacecraft Measurements for the 1 May 1998 Shock

Spacecraft	ϕ (deg)	θ (deg)	V_S (km/s)
Wind	179.0 ± 1.3	6.0 ± 0.8	640.8 ± 2.0
ACE	219.8 ± 2.1	3.4 ± 2.4	532.7 ± 7.0
Geotail	197.4 ± 2.7	−6.3 ± 2.8	618.7 ± 10.3
IMP 8	174.9 ± 2.5	−28.4 ± 2.9	581.2 ± 10.8

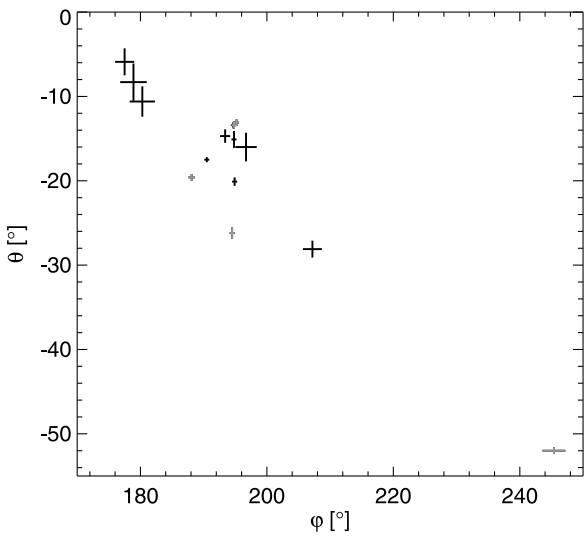

Figure 4. Shock normals calculated from four-spacecraft times and locations of the 1 May 1998 shock observations. The bar length indicates uncertainty.

one hand and Geotail, IMP 8, Interball-1, and SOHO on the other. The much greater difference between the local normals (β angle) for the Wind-Geotail and Wind-IMP 8 pairs may indicate local curvature at the locations of Geotail and IMP 8. This is in agreement with a significant difference between the Geotail and IMP 8 local normals (Table 2) in spite of the relatively small separation between these spacecraft. For the Wind-ACE pair, however, the high α angle is consistent with the β angle, which suggests almost constant curvature between the Wind and ACE locations. Comparison of the local Wind and ACE normals (Table 2) shows that this curvature is almost completely in the XY_{GSE} plane.

[18] Finally, it should be pointed out that the shock parameter determination from the magnetic field and plasma measurements depends on correct choice of upstream and downstream intervals that best represent the shock, which is especially difficult in the case of highly changing measurements, and on the accuracy of plasma measurements, which may differ on different spacecraft. Therefore, the obtained results of the shock curvature can serve as a qualitative picture of complex shock shape rather than being the precise quantitative values of the shock curvature. However, the observed deviation from planarity on the separation between the spacecraft cannot be explained only by error in the calculated local shock parameters since the deviation from planarity is clearly visible from differences between the four-spacecraft normals calculated from times and locations of shock observations by spacecraft, where the uncertainty for each spacecraft, except for IMP 8, is well known.

3. IP Shock Shapes

[19] We have analyzed 62 fast forward IP shocks observed by Wind and at least one other spacecraft in the solar wind from 1995 to 1999 to systematically estimate the shock curvatures on the scales of spacecraft separations. The times of the shock observations by Wind together with the Wind local shock normals and speeds calculated using the *Viñas and Scudder* [1986] and *Szabo* [1994] technique are shown in Table 4.

[20] The 3DP instrument, due to its high time resolution (3 s), allows choosing upstream and downstream intervals that are close to the shock ramp and are very short (~30 s), thus satisfying the condition that both intervals are measured almost simultaneously. The SWE instrument, on the other hand, while having lower time resolution (92 s) resulting in longer (~15 min) selected upstream and downstream intervals, is expected to have higher accuracy in the calculated plasma parameters. To take advantage of both sets of observations, the measurements of both 3DP and SWE instruments were used in the calculating the local shock normals and speeds, and Table 4 contains both results. Since it is well known that the 3DP instrument may provide shifted proton density measurements compared to those of the SWE instrument, we normalized the 3DP density to the SWE value for each event where the measurements of both instruments were available and a difference between 3DP and SWE densities was observed. A higher number of cases with fits results based on 3DP observations results from better coverage of the 3DP data and from a number of shocks with significant changes in the observed magnetic field or plasma parameters close to the shock ramp that precluded using the SWE data.

[21] A comparison of the 3DP and SWE based solutions indicates a difference in the shock normals with a mean of 11°. This difference can be attributed to the different time intervals used upstream and downstream for the analysis and to the different accuracies of the instrument measurements. We have also compared the SWE based solutions in our list with the online database of IP shocks (http://www.cfa.harvard.edu/shocks/) maintained by J. Kasper. For the 34 compared shocks, the angles between the normals are generally in the range form ~5° to ~15°; however, there are several cases with significantly higher differences. We believe that the higher differences are mainly caused by the automated selection of upstream and downstream intervals for the analysis in the online database. It should also be noted that our shock list partly overlaps with the list presented by *Berdichevsky et al.* [2000, 2001]. For the five overlapping shocks where the solutions using the SWE data are available in our list, there is a difference in the shock normals between the lists with a mean of 6°. This differences can partly be due to slightly different time intervals selected for the analysis and partly to the difference in the number of RH equations used.

[22] To estimate the shock curvatures on different scales we used the same technique as the one in section 2 for the 1 May 1998 shock. The technique uses the local shock normal and speed calculated at Wind together with the

Table 3. Normal Differences Between Wind and Other Spacecraft for the 1 May 1998 Shock[a]

Spacecraft	$t_{obs} - t_{pred}$ (s)	$R_\perp$ (R_E)	α (deg)	β (deg)
ACE	247	54.8	48.8	40.8
Geotail	12	50.4	3.1	22.3
IMP 8	58	71.1	9.2	34.7
Interball-1	−20	39.4	6.1	—
SOHO	−34	80.4	5.2	—

[a]See text for details.

Table 4. Local Normal Directions in GSE Coordinates and Speeds at Wind Calculated Using the 3DP and SWE Data for the Analyzed IP Shocks[a]

			3DP			SWE		
Date	Time	Index	ϕ (deg)	θ (deg)	V_S (km/s)	ϕ (deg)	θ (deg)	V_S (km/s)
19950417[b]	2333:07	8	181.5 ± 3.2	32.6 ± 2.2	395.4 ± 6.6			
19950724	0223:12	1	216.0 ± 1.4	7.2 ± 2.5	370.5 ± 2.6	213.1 ± 1.1	6.3 ± 2.2	365.1 ± 2.0
19950824	2211:04	14	178.3 ± 1.0	−30.0 ± 0.9	372.3 ± 2.5	189.3 ± 2.4	−29.9 ± 2.0	344.8 ± 5.4
19960206	1914:22	88	200.1 ± 1.2	34.2 ± 0.6	336.7 ± 1.7			
19960302	2031:51	99	162.3 ± 4.4	77.0 ± 1.3	112.5 ± 2.5	181.6 ± 0.6	69.1 ± 0.9	145.2 ± 2.0
19960618	2235:57	1	185.7 ± 1.7	10.5 ± 2.0	471.2 ± 2.9	170.9 ± 3.8	8.2 ± 4.7	472.3 ± 10.2
19961111	1512:18	5	165.6 ± 0.8	−15.2 ± 0.6	377.9 ± 1.1			
19970410	1258:34	9	153.8 ± 0.9	41.5 ± 0.9	358.8 ± 8.0	159.0 ± 1.5	54.4 ± 1.5	271.0 ± 3.9
19970416	1221:27	58	209.0 ± 0.9	8.3 ± 1.4	388.4 ± 1.9	205.0 ± 1.3	3.3 ± 1.4	382.9 ± 2.5
19970515	0115:22	565	207.8 ± 0.4	−15.8 ± 0.5	427.0 ± 1.6	208.5 ± 0.8	−15.6 ± 1.1	426.0 ± 2.4
19970525	1349:57	56	169.4 ± 1.1	−23.7 ± 1.3	330.3 ± 2.4			
19970526	0909:08	45	198.4 ± 1.3	−25.9 ± 1.1	321.3 ± 1.5			
19970805	0459:05	5	204.4 ± 1.3	5.7 ± 1.5	404.6 ± 2.5	215.2 ± 6.2	−2.3 ± 6.8	332.9 ± 9.1
19970902	2237:38	164	206.9 ± 0.6	−15.3 ± 0.5	371.6 ± 1.4			
19970903	0838:39	44	161.8 ± 1.0	−11.9 ± 0.8	421.1 ± 2.1			
19971010	1557:06	5	177.7 ± 0.6	24.2 ± 0.5	471.8 ± 2.6	186.2 ± 2.3	36.0 ± 2.4	409.9 ± 10.4
19971024	1118:09	91	200.8 ± 1.3	9.8 ± 1.2	493.3 ± 3.5			
19971101	0614:45	5	195.7 ± 0.4	−20.9 ± 0.4	367.9 ± 1.5	198.3 ± 3.2	−27.7 ± 2.5	339.6 ± 6.8
19971109	2222:57	1	170.9 ± 1.7	32.7 ± 0.6	363.5 ± 1.5			
19971122	0912:53	5	189.2 ± 0.5	12.8 ± 1.2	483.9 ± 3.3			
19971130	0715:44	48	194.8 ± 0.8	29.1 ± 1.0	326.7 ± 1.7	198.3 ± 2.0	32.4 ± 1.1	308.7 ± 2.6
19971230	0113:44	1	199.2 ± 0.6	−25.5 ± 0.6	402.2 ± 1.7			
19980106	1329:00	18	158.9 ± 0.6	20.3 ± 0.6	386.6 ± 1.2			
19980304	1102:46	5	173.9 ± 2.2	−12.8 ± 1.5	433.3 ± 2.2			
19980407	1653:34	8	178.3 ± 1.7	−37.5 ± 0.5	306.1 ± 1.2	174.9 ± 2.2	−32.7 ± 1.5	360.4 ± 4.3
19980501	2121:24	451	190.0 ± 2.4	−3.8 ± 2.1	645.1 ± 5.3			
19980515	1353:46	64	205.5 ± 0.4	−11.3 ± 0.4	383.4 ± 0.9	210.9 ± 0.9	−13.1 ± 1.0	359.0 ± 1.7
19980613	1918:12	5	120.7 ± 1.4	−12.4 ± 1.5	254.9 ± 3.7	122.8 ± 2.0	−8.4 ± 1.5	277.0 ± 6.8
19980806	0716:07	51	189.4 ± 0.5	3.2 ± 0.6	497.2 ± 1.5	171.7 ± 1.9	24.7 ± 2.2	440.9 ± 8.4
19980810	0031:15	965	220.3 ± 2.0	46.2 ± 3.1	312.2 ± 5.2			
19980819	1840:41	56	214.9 ± 1.7	−18.3 ± 0.8	303.1 ± 1.5	208.2 ± 1.8	−21.1 ± 1.6	308.1 ± 2.1
19980822	0211:18	85	235.3 ± 0.6	−20.3 ± 0.6	239.8 ± 1.4	236.1 ± 1.1	−11.4 ± 1.0	231.0 ± 2.0
19980826	0640:25	55	181.5 ± 1.1	−43.4 ± 0.8	598.7 ± 5.6			
19980924	2320:37	555	198.6 ± 1.2	−23.4 ± 2.7	696.0 ± 17.4			
19981002	0706:02	18	139.5 ± 2.8	5.1 ± 3.8	664.2 ± 8.6			
19981023	1258:21	94	170.6 ± 5.9	−65.4 ± 1.7	344.1 ± 4.6			
19981108	0441:18	5	154.2 ± 2.0	−22.2 ± 2.5	694.7 ± 17.1			
19981226	0956:30	8	112.7 ± 4.6	−69.0 ± 1.6	198.1 ± 4.8	128.9 ± 3.3	−66.2 ± 1.4	262.4 ± 6.9
19981228	1820:17	4	198.1 ± 1.3	−10.8 ± 1.1	465.5 ± 2.7			
19990113	1047:43	81	169.6 ± 3.4	21.1 ± 2.4	396.7 ± 3.8	171.5 ± 3.1	9.3 ± 4.7	409.0 ± 8.1
19990122	2021:45	9	160.9 ± 3.8	3.0 ± 3.3	653.8 ± 18.4	174.4 ± 5.6	−14.8 ± 5.5	695.5 ± 22.8
19990217	0712:13	9	173.5 ± 0.9	−4.5 ± 1.4	556.3 ± 2.8	174.3 ± 2.9	−17.1 ± 4.4	535.1 ± 7.4
19990218	0248:15	5	182.9 ± 3.1	−6.6 ± 2.5	706.5 ± 16.6			
19990228	2142:51	5	181.1 ± 1.8	−3.3 ± 2.1	452.6 ± 2.7	168.1 ± 1.5	−21.3 ± 1.6	400.5 ± 5.3
19990310	0133:01	555	187.9 ± 1.1	10.3 ± 1.1	508.2 ± 2.9	190.2 ± 1.9	12.0 ± 2.1	480.9 ± 2.7
19990416	1114:00	91	150.2 ± 3.8	24.2 ± 2.3	402.2 ± 8.2			
19990518	0032:40	61	179.0 ± 1.4	−2.3 ± 1.5	435.2 ± 1.7	187.9 ± 0.8	−1.1 ± 0.6	439.3 ± 1.3
19990626	0231:39	454	199.3 ± 0.7	3.8 ± 0.6	406.6 ± 2.1	201.2 ± 0.7	−0.4 ± 0.9	373.9 ± 1.7
19990626	1931:05	4	195.7 ± 1.4	9.8 ± 1.7	439.8 ± 4.7	174.9 ± 1.2	9.4 ± 1.0	453.4 ± 4.6
19990706	1424:57	588	194.2 ± 1.7	31.1 ± 1.1	429.8 ± 3.6	183.9 ± 1.8	−3.8 ± 1.7	481.7 ± 7.4
19990726	2350:17	5	195.0 ± 1.3	30.8 ± 1.7	428.3 ± 3.3			
19990804	0144:37	256	191.7 ± 0.7	−16.3 ± 1.0	402.6 ± 1.6	185.2 ± 2.1	−24.7 ± 2.0	404.6 ± 3.5
19990815	1033:46	55	174.0 ± 0.8	−18.9 ± 0.8	402.1 ± 1.2	171.8 ± 1.4	−9.8 ± 2.5	418.1 ± 2.2
19990823	1211:15	42	197.5 ± 0.9	3.0 ± 1.0	479.6 ± 3.3	190.8 ± 2.3	−8.4 ± 2.6	469.1 ± 4.7
19990823	1541:33	2	187.3 ± 1.2	−9.2 ± 1.4	529.6 ± 3.8	191.6 ± 2.8	−23.0 ± 4.2	482.8 ± 11.2
19990912	0357:55	911	217.9 ± 1.9	15.2 ± 1.3	442.8 ± 3.0			
19990915	0743:46	55	182.2 ± 2.3	14.8 ± 3.5	681.5 ± 11.8			
19990915	2008:37	5	204.4 ± 2.5	22.2 ± 2.3	581.9 ± 6.8			
19990922	1209:25	866	182.7 ± 1.8	40.3 ± 1.1	455.2 ± 2.9			
19991021	0220:52	55	183.8 ± 0.7	19.1 ± 0.8	463.9 ± 1.9	187.3 ± 2.0	23.5 ± 1.9	462.7 ± 4.4
19991105	2003:09	95	155.5 ± 0.9	−18.2 ± 0.8	367.8 ± 2.2	155.1 ± 2.0	−13.8 ± 1.3	376.5 ± 3.2
19991113	1248:57	94	151.3 ± 0.5	−9.0 ± 0.3	472.2 ± 2.0	148.6 ± 1.3	−4.4 ± 0.9	445.2 ± 2.8

[a]See text for details.
[b]Read 19950417 as 17 April 1995.

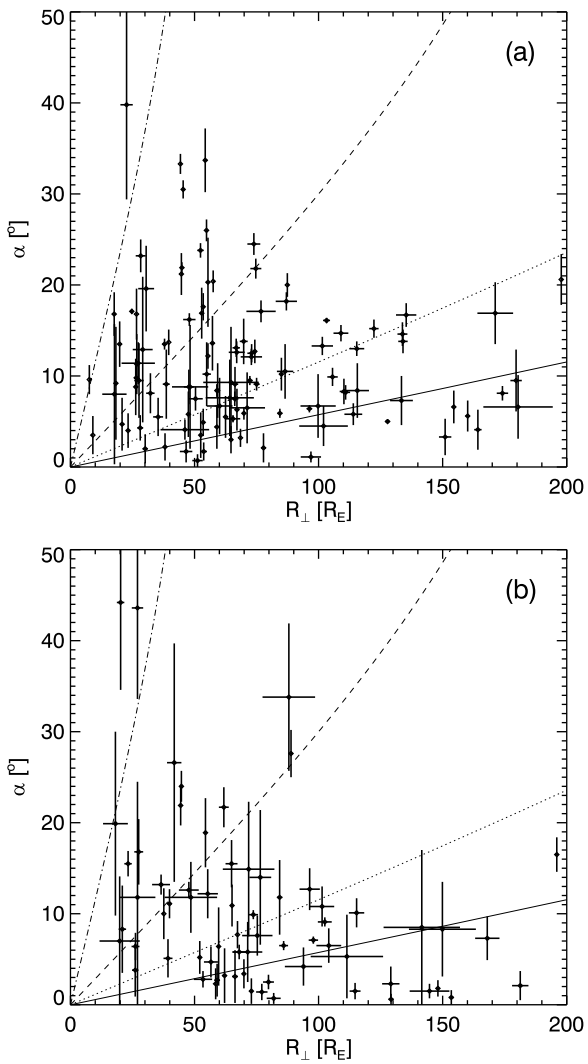

Figure 5. Normal differences between Wind and other spacecraft calculated using (a) Wind 3DP and (b) SWE data as a function of distance perpendicular to the Wind local shock normal. Solid, dotted, dashed, and dot-dashed lines indicate the model normal differences corresponding to shock curvatures of 1000, 500, 200, and 50 R_E, respectively. See text for details.

times and locations of the shock observations by Wind and another spacecraft. It calculates, under assumption of constant shock curvature on the scale length of inter-spacecraft separation, the radius of curvature or, equivalently, the angle between the normals at the two locations on the shock surface. Figure 5 shows the angle between the normals at two locations on the shock surface calculated separately using the Wind 3DP (Figure 5a) and SWE (Figure 5b) data as a function of distance perpendicular to the Wind local shock normal. The horizontal and vertical bars at each point indicate the uncertainties in the corresponding parameters. The uncertainty in the angle between the normals results from the uncertainties in the calculated Wind shock normal and speed and the uncertainties in the times and locations of the shock observations by spacecraft, while the uncertainty in the distance perpendicular to the Wind local shock normal results from the uncertainty in the calculated Wind shock normal and the uncertainties in the locations of the shock observations by the spacecraft. Solid, dotted, dashed, and dot-dashed lines in Figure 5 indicate the model normal differences corresponding to constant shock curvatures of 1000, 500, 200, and 50 R_E, respectively.

[23] To interpret the results presented in Figure 5, it should be pointed out that a nonzero angle between the normals can result from either constant shock curvature on the scale of separation between two spacecraft or from a local curvature at Wind on a scale smaller than the spacecraft separation. In the latter case, the calculated constant curvature on the scale of spacecraft separation will generally be overestimated; however, this will also imply a stronger than calculated local curvature at Wind. As can be seen from Figure 5a, on scales up to ~30 R_E the calculated angles between the normals correspond to the shock curvature radii in the range from ~50 to ~500 R_E, with the majority of cases in the range from ~50 to ~200 R_E. As mentioned above, the same observations can be produced by stronger local curvatures at Wind, and thus the obtained results can serve as lower limits of the shock curvatures on small scales. For the scales from ~30 to ~100 R_E most of the cases correspond to shock curvature radii in the range from ~200 to ~1000 R_E and for the scales from ~100 R_E all cases correspond to shock curvature radii greater than ~400 R_E. The influence of local shock curvature at Wind on the calculated angle between the normals and the presence of small-scale curvatures with radii of less than ~50 to ~200 R_E, as demonstrated above, indicate that the obtained shock curvatures on larger scales are generally overestimated and can only serve as upper limits of possible curvatures on these scales. The results obtained using the SWE data (Figure 5b) show a similar pattern, with slightly smaller angles between the normals at larger scales compared to the 3DP results. The correspondence between the results in Figure 5 and the shocks listed in Table 4 is provided by the index column in Table 4. Each digit in the column corresponds to one spacecraft pair used to calculate the normal difference. For each digit, triplets 1–3, 4–6, and 7–9 are used to separate the spacecraft perpendicular separation into <30 R_E, 30 to 100 R_E, and >100 R_E, respectively. Inside the triplets, digits from the lowest to the highest correspond to the radii of curvature of <200 R_E, 200 to 1000 R_E, and >1000 R_E, respectively.

[24] *Neugebauer and Giacalone* [2005] used the same two-spacecraft technique and ACE as the main spacecraft to analyze the curvatures of 26 IP shocks. Their results of the shock radii of curvature are in the range of 3×10^5 to 10^7 km, which are similar to the results of our study. However, we would like to point out that these results have to be interpreted together with the scales on which they were obtained: on small scales the results are the lower limits of the local shock curvatures at the main spacecraft while on larger scales they are the stronger limits of possible curvatures on these scales.

4. Summary

[25] We have analyzed in detail an IP shock on 1 May 1998 observed by six spacecraft in the solar wind. The shock parameters were calculated at the locations of four spacecraft using the *Viñas and Scudder* [1986] and *Szabo*

[1994] technique. The calculated local normals indicate significant differences between the shock orientations at different locations. To differentiate between global shock curvature and local ripples on the shock surface, we estimated the shock curvature as a function of the separation distances between Wind and other spacecraft. Our results suggest that on the scale of separation between Wind on the one hand and Geotail, IMP 8, Interball-1, and SOHO on the other the shock shape may be close to planarity. The much greater difference between the local normals for the Wind-Geotail and Wind-IMP 8 pairs may indicate local curvature at the locations of Geotail and IMP 8. For the Wind-ACE pair, however, the high difference between the local normals is consistent with an almost constant shock curvature on the scale of the spacecraft separation. This curvature is almost completely in the XY_{GSE} plane.

[26] To systematically estimate the shock front deviation from planarity on different scales, we have analyzed 62 IP shocks observed by Wind and at least one other spacecraft in the solar wind. The calculated shock local parameters at Wind together with the times and locations of the shock observations by two spacecraft were used to estimate the curvatures on the scales of spacecraft separations. Our results show the presence of local (on scales up to ~30 R_E) shock curvatures with radii of less than ~50 to ~200 R_E for the majority of analyzed shocks. On larger scales, the shock curvature decreases and reaches the limit of the strongest possible curvature with radius of ~400 R_E on scales greater than ~100 R_E for all analyzed shocks.

[27] **Acknowledgments.** The authors acknowledge the CDAWeb data source for the provided spacecraft data.

[28] Philippa Browning thanks Zdenek Nemecek and another reviewer for their assistance in evaluating this paper.

References

Abraham-Shrauner, B. (1972), Determination of magnetohydrodynamic shock normals, *J. Geophys. Res.*, *77*, 736–739.

Abraham-Shrauner, B., and S. H. Yun (1976), Interplanetary shocks seen by AMES plasma probe on Pioneer 6 and 7, *J. Geophys. Res.*, *81*, 2097–2102.

Bellomo, A., and A. Mavretic (1978), Description of the MIT plasma experiment on IMP 7/8, *Rep. CSR TR-78-2*, p. 51, Cent. for Space Res., Mass. Inst. of Technol., Cambridge.

Berdichevsky, D. B., A. Szabo, R. P. Lepping, A. F. Viñas, and F. Mariani (2000), Interplanetary fast shocks and associated drivers observed through the 23rd solar minimum by Wind over its first 2.5 years, *J. Geophys. Res.*, *105*, 27,289–27,314, doi:10.1029/1999JA000367.

Berdichevsky, D. B., A. Szabo, R. P. Lepping, A. F. Viñas, and F. Mariani (2001), Erratum: "Interplanetary fast shocks and associated drivers observed through the 23rd solar minimum by Wind over its first 2.5 years," *J. Geophys. Res.*, *106*, 25,133–25,134, doi:10.1029/2001JA000074.

Colburn, D. S., and C. P. Sonett (1966), Discontinuities in the solar wind, *Space Sci. Rev.*, *5*, 439.

Frank, L. A., K. L. Ackerson, W. R. Paterson, J. A. Lee, M. R. English, and G. L. Pickett (1994), The Comprehensive Plasma Instrumentation (CPI) for the Geotail spacecraft, *J. Geomagn. Geoelectr.*, *46*, 7–21.

Ipavich, F. M., et al. (1998), Solar wind measurements with SOHO: The CELIAS/MTOF proton monitor, *J. Geophys. Res.*, *103*, 17,205–17,214, doi:10.1029/97JA02770.

Jeřáb, M., Z. Němeček, J. Šafránková, K. Jelínek, and J. Měrka (2005), Improved bow shock model with dependence on the IMF strength, *Planet. Space Sci.*, *53*, 85–93, doi:10.1016/j.pss.2004.09.032.

Kokubun, S., T. Yamamoto, M. H. Acuna, K. Hayashi, K. Shiokawa, and H. Kawano (1994), The Geotail magnetic field experiment, *J. Geomagn. Geoelectr.*, *46*, 7–21.

Koval, A., and A. Szabo (2008), Modified "Rankine-Hugoniot" shock fitting technique: Simultaneous solution for shock normal and speed, *J. Geophys. Res.*, *113*, A10110, doi:10.1029/2008JA013337.

Lepping, R. P., and P. D. Argentiero (1971), Single spacecraft method of estimating shock normals, *J. Geophys. Res.*, *76*, 4349–4359.

Lepping, R. P., et al. (1995), The Wind Magnetic Field Investigation, *Space Sci. Rev.*, *71*, 207–229.

Lin, R. P., et al. (1995), A three-dimensional plasma and energetic particle investigation for the Wind spacecraft, *Space Sci. Rev.*, *71*, 125–153.

McComas, D. J., S. J. Bame, P. Barker, W. C. Feldman, J. L. Phillips, P. Riley, and J. W. Griffee (1998), Solar Wind Electron Proton Alpha Monitor (SWEPAM) for the Advanced Composition Explorer, *Space Sci. Rev.*, *86*, 563–612.

Mish, W. H., and R. P. Lepping (1976), Magnetic field experiment data processing systems: Explorers 47 and 50, *Internal Publ. X-694-76-158*, NASA Goddard Space Flight Cent., Greenbelt, Md.

Neugebauer, M., and J. Giacalone (2005), Multispacecraft observations of interplanetary shocks: Nonplanarity and energetic particles, *J. Geophys. Res.*, *110*, A12106, doi:10.1029/2005JA011380.

Neugebauer, M., J. Giacalone, E. Chollet, and D. Lario (2006), Variability of low-energy ion flux profiles on interplanetary shock fronts, *J. Geophys. Res.*, *111*, A12107, doi:10.1029/2006JA011832.

Ogilvie, K. W., et al. (1995), SWE, A comprehensive plasma instrument for the Wind spacecraft, *Space Sci. Rev.*, *71*, 55–77.

Petrinec, S. M., and C. T. Russell (1996), Near-Earth magnetotail shape and size as determined from the magnetopause flaring angle, *J. Geophys. Res.*, *101*, 137–152, doi:10.1029/95JA02834.

Pulupa, M., and S. D. Bale (2008), Structure on interplanetary shock fronts: Type II radio burst source regions, *Astrophys. J.*, *676*, 1330–1337, doi:10.1086/526405.

Russell, C. T., M. M. Mellott, E. J. Smith, and J. H. King (1983a), Multiple spacecraft observations of interplanetary shocks: Four spacecraft determination of shock normals, *J. Geophys. Res.*, *88*, 4739–4748.

Russell, C. T., J. T. Gosling, R. D. Zwickl, and E. J. Smith (1983b), Multiple spacecraft observations of interplanetary shocks ISEE three-dimensional plasma measurements, *J. Geophys. Res.*, *88*, 9941–9947, doi:10.1029/JA088iA12p09941.

Russell, C. T., et al. (2000), The interplanetary shock of September 24, 1998: Arrival at Earth, *J. Geophys. Res.*, *105*, 25,143–25,154, doi:10.1029/2000JA900070.

Šafránková, J., G. Zastenker, Z. Němeček, A. Fedorov, M. Simersky, and L. Přech (1997), Small scale observation of magnetopause motion: Preliminary results of the INTERBALL project, *Ann. Geophys.*, *15*, 562–569.

Smith, C. W., J. L'Heureux, N. F. Ness, M. H. Acuña, L. F. Burlaga, and J. Scheifele (1998), The ACE Magnetic Fields Experiment, *Space Sci. Rev.*, *86*, 613–632.

Szabo, A. (1994), An improved solution to the 'Rankine-Hugoniot' problem, *J. Geophys. Res.*, *99*, 14,737.

Szabo, A. (2005a), Determination of interplanetary shock characteristics, in *Proceedings of the Conference Solar Wind 11 – SOHO 16*, *ESA Spec. Publ.*, *SP-592*, 449–452.

Szabo, A. (2005b), Multi-spacecraft observations of interplanetary shocks, in *The Physics of Collisionless Shocks: 4th Annual IGPP International Astrophysics Conference*, *AIP Conf. Ser.*, vol. 781, edited by G. Li, G. P. Zank, and C. T. Russell, pp. 37–41, doi:10.1063/1.2032672, Am. Inst of Phys., New York.

Szabo, A., R. P. Lepping, J. Merka, C. W. Smith, and R. M. Skoug (2001), The evolution of interplanetary shocks driven by magnetic clouds, in *Solar Encounter: Proceedings of the First Solar Orbiter Workshop*, *ESA Spec. Publ.*, *SP-493*, 383–387.

Terasawa, T., et al. (2005), Determination of shock parameters for the very fast interplanetary shock on 29 October 2003, *J. Geophys. Res.*, *110*, A09S12, doi:10.1029/2004JA010941.

Viñas, A. F., and J. D. Scudder (1986), Fast and optimal solution to the "Rankine-Hugoniot problem," *J. Geophys. Res.*, *91*, 39–58.

A. Koval and A. Szabo, Heliospheric Physics Laboratory, NASA Goddard Space Flight Center, Mail Code 672, 8800 Greenbelt Rd., Greenbelt, MD 20771, USA. (andriy.koval@nasa.gov; adam.szabo@nasa.gov)